Design of Submerged Air-Intake for UAV Application

Kishan Tanna[1*], Niyati Shah[2], Mr. Vinay Kumar Bommoju[3]

*[*1]Graduate Student*
Aeronautical Engineering Department, Sardar Vallabhbhai Patel Institute of Technology, Vasad, Anand, India

[2]Assistant Professor
Aeronautical Engineering Department, Sardar Vallabhbhai Patel Institute of Technology, Vasad, Anand, India

[3]Manager - Aerodynamics
Hindustan Aeronautics Limited, Nashik.

[*]Corresponding Author
Kishan Tanna, Aeronautical Engineering Department, Sardar Vallabhbhai Patel Institute of Technology, Vasad, Anand, India.

Citation: Tanna, K., Shah, N., Bommoju, V. K. (2023). Design of Submerged Air-Intake for UAV Application. *OA J Applied Sci Technol, 1*(2), 89-103.

Abstract
The design approach and performance analysis of a custom s-duct submerged inlet are presented in this paper for a stealth subsonic swept-back Unmanned Aerial Vehicle (UAV). The UAV must provide good efficiency in a wider range of operating conditions. The duct is designed in such a way that it is the best compromise between the fuselage-engine framework and should provide maximum pressure recovery. Important geometric parameters of the s-duct inlet consist of a length-to-engine diameter ratio of 5.18, an offset-to-length ratio of 0.12, and an area ratio of 1.89. A review of fundamental concepts and the design process is presented to provide a foundation for future design iterations. METACOMP CFD++ software has been used to analyze the inlet design performance. Pressure recovery and circumferential total pressure distortion are used to analyze inlet performance at zero incidence angle.

Keywords: Submerged Air Intake; S-Duct Designing; Computational Fluid Dynamics; Inlet Design Aerodynamics, Pressure Recovery, Total Pressure Distortion; Unmanned Aerial Vehicles

1. Introduction

The design of intakes for high-performance Unmanned Aerial Vehicles (UAVs) is a complex task, as these vehicles combine the characteristics of high-performance agile aircrafts on one hand and missiles with air-breathing propulsion on the other. Several conflicting targets have to be accomplished, such as good efficiency, in terms of high-pressure recovery and low-pressure distortion, low drag, and high margins of stability. The above-mentioned characteristics should be maintained throughout a wide range of operating conditions, such as different flight Mach numbers, angles of incidence, sideslip, and engine thrust, while, at the same time, cost, and complexity should be maintained as low as possible. An S-Duct is a form of air intake located in the aircraft's upper or lower rear. This design makes a shorter fin and a rudder closer to the longitudinal axis possible. Separated flow and complex shock boundary layer interactions, sometimes unstable, will be present throughout a wide range of flying conditions due to the S-type shape of the intakes. Furthermore, all of the foregoing should be evaluated in the context of the airflow interactions between the fuselage, wing, intake, and engine. Inlet aerodynamic design differs from external aerodynamic design in the fundamental sense that inlets must operate constantly in separated flow regimes, whereas external aerodynamic design frequently employs flow separation as a limit of operation. In consideration of the entire mission profile, an efficient intake design efficiently balances the delivery of clean airflow to the engine with the consequence of external drag on the aircraft. To achieve supersonic flight, an engine implanted inside the fuselage was required to reduce rapid increases in drag during transonic flight. The key parameters of concern after World War II were the study behavior of shock waves, shock interactions, pressure recovery, and dynamic distortion. In the late 1970s, the swirling flow on compressor surge issue was identified. An effective intake design often depends on balancing the requirements of the internal and external flow fields [1]. Apart from the experimental work, the CFD analysis of S-duct inlets has been performed and reported in the literature. These studies focused on the effects of centerline curvature, length, offset, flow turning angle, cross-sectional shape, incidence angle, and boundary layer ingestion on pressure recovery and flow distortion at the Aerodynamic Interface Plane (AIP). Time-variant flow behavior in diffusing s-duct inlets

has also been predicted using higher-order computational models.

To evaluate the impacts of centerline curvature and transitioning cross-sections in complex inlet designs, employed a parabolic three-dimensional Navier-Stokes CFD system. The centerline offset and the thickness of the boundary layer at the diffuser entrance were found to be the main causes of distortion at the AIP [2]. It was discovered that the transition of diffuser cross-sections had a secondary influence on the overall pressure loss in the intake. The effect of flow turning angles and aspect ratio for s- s-shaped rectangular diffusers was investigated by using CFD tools [3]. It was observed that flow homogeneity diminished and cross-flow velocities rose with the increase in flow turning angles from 15°/15°, 22.5°/22.5°, 45°/45° to 90°/90°. used Reynolds-Averaged Navier–Stokes (RANS) simulations with several turbulence models to evaluate the RAE-M2129 inlet's performance at various pitch and yaw angles [4]. The positive angles of yaw revealed a reduction in inlet distortion and an increase in pressure recovery because of the reduced influence of offset. Negative yaw angles amplified the effect of offset, resulting in decreased inlet performance. Four flush-mounted S-duct inlet geometries were evaluated for performance using experimental and computational techniques by for a variety of Mach values and with significant amounts of boundary layer ingestion [5]. Mach numbers from 0.25 to 0.83 were used for the tests. To depict the computational model, steady-state RANS equations were solved, and k-Shear Stress Transport (SST) was employed to simulate turbulence. Results showed that particularly at low Mach number regions, pressure recovery generally reduced and distortion increased with increasing Mach number.The effects of inlet offset on the performance of an s-duct diffuser with a 90°/90° turn were studied by [6]. The inlet's cross-sectional geometry was lofted between a rectangular inlet and a semi-circular outlet. According to the findings, higher input offset resulted in lower pressure recovery and increased flow non-uniformity at the exit. To analyze an S-duct intake developed for a UAV application, employed RANS equations and a SST two-equation turbulence model [7]. The inlet used Gerlach area shaping to create a loft between a rectangular cross-section with rounded corners and a circular cross-section at the AIP. The bespoke s-duct was engineered for a free-stream Mach number of 0.85 at 6,000 meters and a mass flow rate of 1.38 kg per second. The inlet was designed with an offset equal to two times the engine face diameter, an area ratio of 1.782, and a length-to-engine face diameter ratio ranging from 0.8 to 1.7. Due to frictional losses, the nearly doubling of input length resulted in a 1.5 percent drop in pressure recovery; nevertheless, there was an extra benefit in terms of flow distortion at the AIP.

3-D RANS equations and a k-based SST model were employed by to evaluate the effects of varying cross-sectional shapes on the RAE-M2129 intake geometry [8]. Cross-sections with upper-half semi-circular and lower-half semi-circular shapes were studied in a total of 21 test cases that varied the aspect ratio. Pressure recovery and distortion were used as performance indicators. The study used a flight Mach number of 0.21 at zero angle of attack and a huge mass flow ratio of 23.245. The results revealed that the upper-half semi-circular shapes performed best, whereas the circular case performed worst. A computational study on engine surge was also done to evaluate the RAE-M2129 inlet's performance, but no experimental data were available for validation [9,10].

In this work, a specific type of S-Duct with a rectangular intake and a circular outlet for a UAV is presented. High-performance UAVs require the adoption of a jet engine to achieve a high subsonic maximum speed. The objective of this work is to design a S-duct intake for a maximum flight Mach Number 0.85 at 6000 m, for a specified engine mass flow rate M˙ of 6.65 kg/s. It was also a mandate to maintain the design Mach number at the compressor's face Me at 0.318. CFD analysis is carried out to find the pressure recovery and total pressure distortion for the aforementioned requirements.

2. Air Intake System Design Procedure
2.1 Inlet design
Turbojet engines are incapable of efficient operation unless the air entering them is slowed to a speed of about Mach 0.3-0.4. This is to keep the tip speed of the compressor blades below sonic speed relative to the incoming air. Slowing down the incoming air is the primary purpose of an inlet system. The installed performance of a jet engine greatly depends upon the air-inlet system. The type and geometry of the inlet and inlet duct will determine the pressure loss and distortion of the air supplied to the engine, which will affect the installed thrust and fuel consumption. As the UAVs are designed to have stealth characteristics, minimum exposure of components outside the fuselage body is a concern for the design. Therefore, a NACA flush inlet is chosen to provide air to the engine. The size of the NACA duct is calculated based on the maximum mass flow rate required by the engine. Table 1 represents the coordinates to design a customized NACA flush inlet based on different mass flow rate requirements. The lengths x, y, w, and L are depicted in Fig. 1: -

x/L	y/(W/2)
1.0	0.083
0.9	0.160
0.8	0.236
0.7	0.313
0.6	0.389
0.5	0.466
0.4	0.614
0.3	0.766
0.2	0.916
0.1	0.996
0.0	1.000

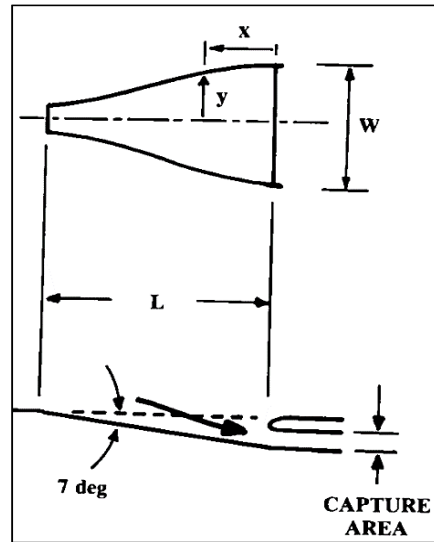**Table 1: NACA Duct Coordinates (*Raymer, 2012*)**

Figure 1: NACA Duct Geometry (*Raymer, 2012*)

The ratio between the engine area and throat area was kept to be 1.89. The engine has an inner radius of 142.993 mm hence the area of the fan face is 64236.1 mm^2. Therefore, the area at the throat comes out to be 33924 mm^2. The width-to-height ratio (w/h) of the rectangular inlet was kept to 2.65 based on the fuselage diameter. The inlet lip profile has an elliptical leading edge with a semi-mi-nor axis of 10 mm. Therefore, the total height of the duct from the fuselage reference line comes out to be 128.62 mm. The ramp of the NACA submerged intake was chosen to be 7°. Hence the length (L1) of the NACA duct comes out to be 1047.526 mm. This length is derived with the help of the Eq. 1.
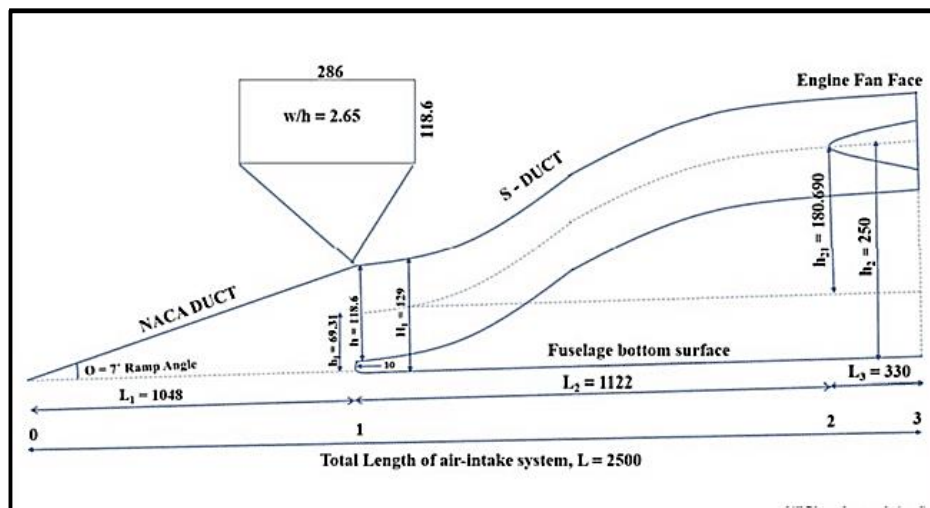
$$L1 = 128.62/\tan(7°) \tag{1}$$

Figure 2: Geometry Sketch

Based on the above data, Fig. 3 represents the CAD model of the NACA Duct:
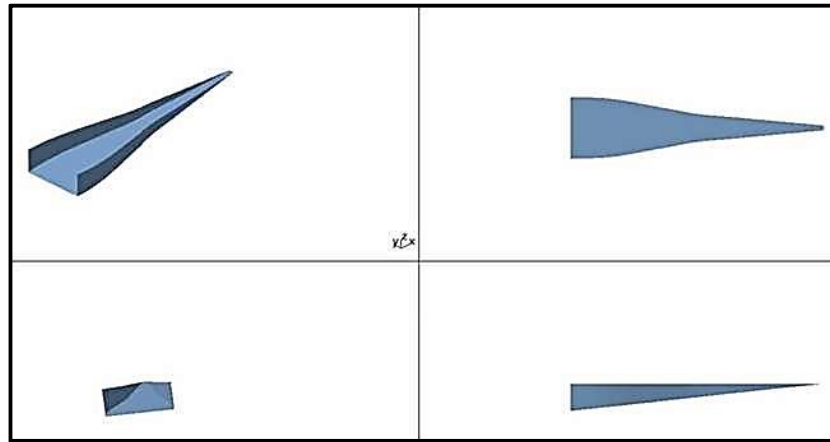
Figure 3: NACA Duct

The lip is inclined downwards at an angle of 2° with reference to the horizontal axis as depicted in Fig. 4, and Fig. 5.
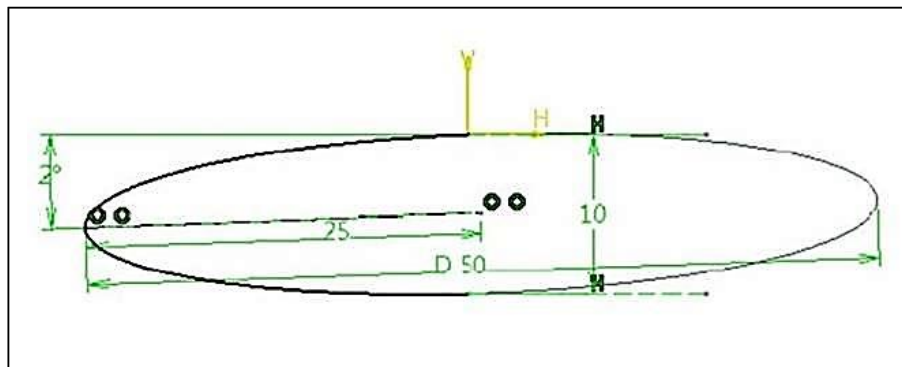
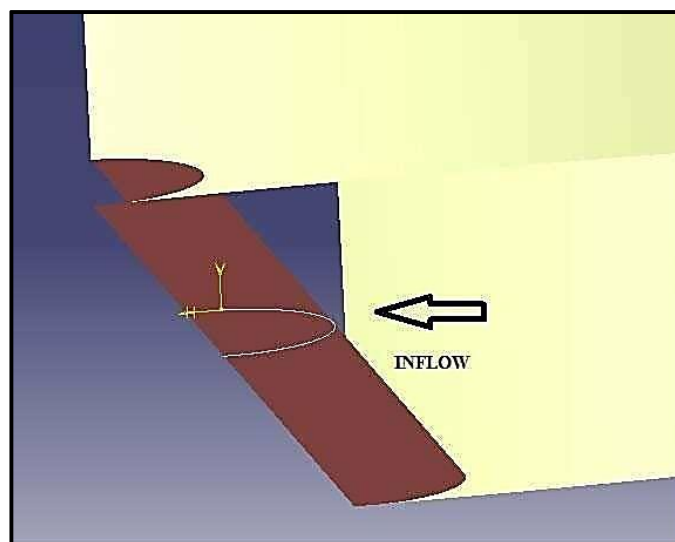

Figure 4: Inlet Lip Geometry

Figure 5: CAD Model of the inlet lip

a. S-Duct Design

The S-Duct is made to fit the engine's diameter and the geometry of the existing fuselage. The duct in this model is built around a reference curve we'll refer to as the centerline. As seen in Fig. 6, the intersection of two circular arcs serves as the foundation for the centerline curvature definition. Since the circles in the illustrated design are all the same size, the radius of curvature changes where the circular arcs overlap. This geometric parameterization has the advantage that Eq. 2 and Eq. 3 make it simple to convert the desired inlet length and offset to an S-Duct centerline.
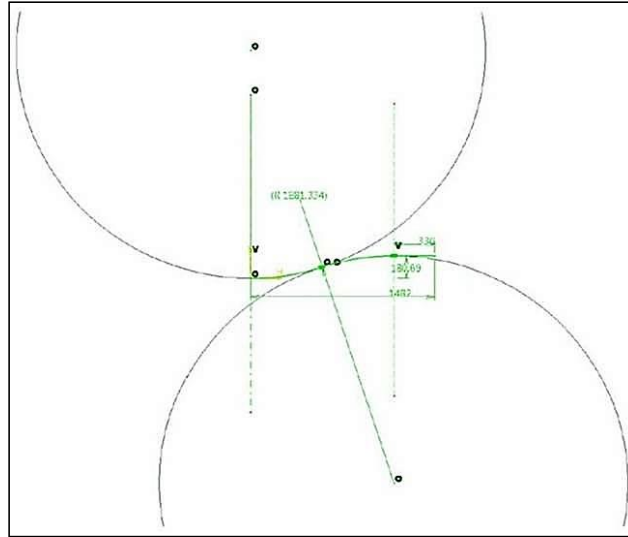

Figure 6: Centre Spline Geometry

$$L = 2R\sin\Theta \tag{2}$$

$$H = 2[1 - \cos\Theta] \tag{3}$$

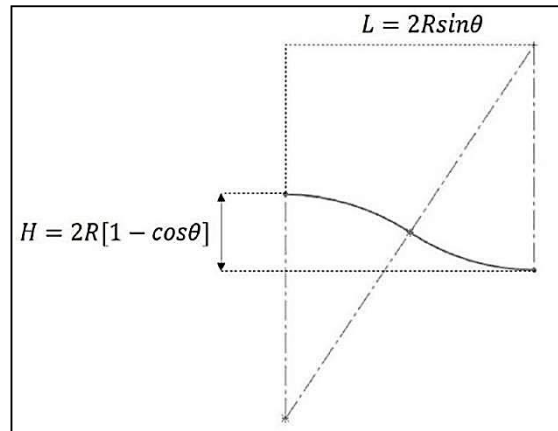These centerline relationships are further illustrated in Fig. 7

Figure 7: Definition of S-Duct Centerline Curvature

There are a range of combinations of circle radius and arc that satisfy each constraint of inlet length and offset, however only one combination of R and Θ exists such that both constraints are met. Along the centerline, several lofting profiles are constructed, at planes normal to the curve. Their positions are non-dimensionally defined as a fraction of the curve's length. In Fig. 8, five such profiles are plotted, of which the first and the last correspond to 0 and 100 percent of the centerline length respectively. The first profile is a rectangular cross-section, which corresponds to the inlet of the S- Duct. The last profile is a circular cross-section, which corresponds to the engine's face. The reason to choose a rectangular cross-section at the throat is to keep the vertical height of the duct as low as possible. The horizontal separation of secondary vortices that this structure can give (as will be shown in the next sections) is another factor in the decision to choose a rectangular cross-section since this results in a more uniform flow field at the com-

pressor's face. The Gerlach Area Shaping Method is used to plot each of these profiles. To materialize Gerlach area shaping for the duct and provide a smooth and controllable area variation between the throat and engine face, three additional profiles are defined in planes normal to the centerline. These profiles correspond to 2, 3, and, 4; their positions are provided as a fraction of the centerline curve's length. The Gerlach area shaping focuses on a range of cross-sections to efficiently lower the transverse pressure gradi-ent and generation of secondary flow by increasing the outer wall velocity and decreasing the inner wall velocity at the first turn. A similar procedure is adopted for the second bend of the S-Duct; however, as the bend is in opposite direction, the narrowing is applied at the inner wall. This is shown in Fig. 8, where the adopted cross-section at the throat (t), engine face (e), and positions 2-4 are presented to illustrate the Gerlach Area Shaping done while designing the duct:
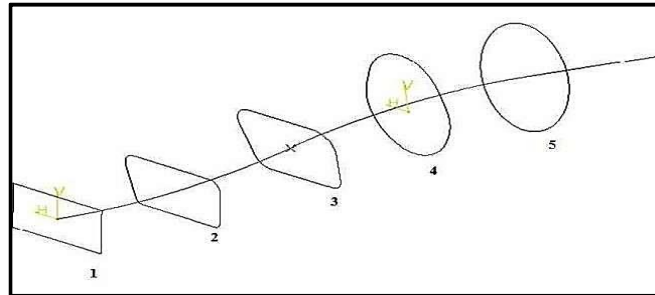

Figure 8: Gerlach Area Geometry

Having the cross-sectional areas specified at the throat, the capture plane, and the engine face plane, the cross-sectional areas of the main duct in the intermediate positions, A2, A3, and A4, respectively, can be specified supposing a smooth variation of area (a smooth diffusion) between the throat and engine face plane. This area variation is shown in the form of area ratios, with respect to the throat area At, while the resulting area ratios are summarized in Table 2 and represented in Fig. 9.

Geometric Parameter	Value
Ae	64236.1 mm^2
At	33923.659 mm^2
A2/ At	1.16
A3/ At	1.44
A4/ At	1.72
Ae/ At	1.89

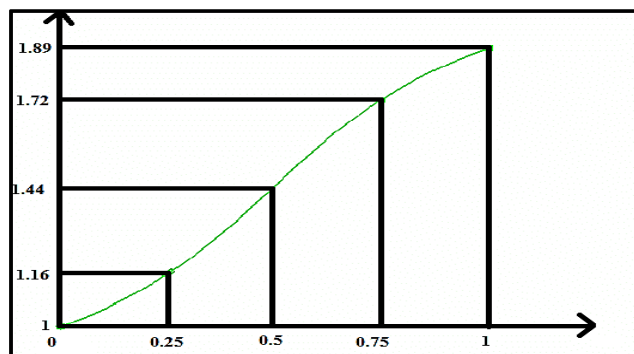**Table 2: Geometric Parameters**

Figure 9: Gerlach Area Variation

The CAD Model of the S-Duct is illustrated in Fig. 10. All these designs are made using CATIA V5 R20 designing software. Multi-Section Solid tool is used to loft the S-Duct geometry.
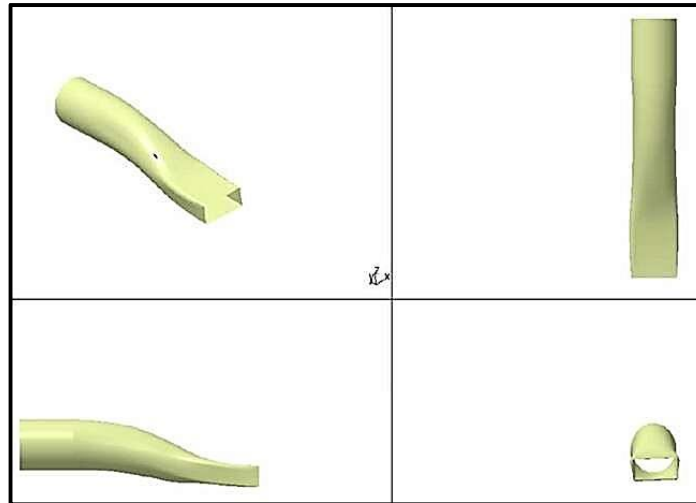

Figure10: CAD Model of S-Duct

CFD analysis has to be carried out to evaluate the performance of the air intake designed in the previous sections. The air intake should provide a maximum mass flow rate of 6.65 kg/s under all conditions. Factors like Pressure Recovery and Pressure Distortion have been analyzed using *METACOMP CFD++* software for the flight conditions depicted in Table 3.

3. Meshing
To evaluate the flight parameters mentioned before, a mesh was generated using *METACOMP MIME 8.1 software*. A fine surface

mesh approximately containing 2.4 million cells and 781,796 nodes is generated over the model. Curvature-based refinement is applied to accurately capture geometry. To accurately capture the flow, a slow volumetric growth rate is applied to the mesh to gradually increase the cell size of prism-shaped boundary layers. A total of 29 prism layers distributed over a total thickness of 9.09×10^{-3} m are used to resolve the boundary layer along with the upstream parallel extension, NACA Duct, inlet lip, and S-Duct. The first cell height is equal to 9.24×10^{-6} m and the y+ value is equal to 1. Different mesh profiles have been depicted in Fig. 11.

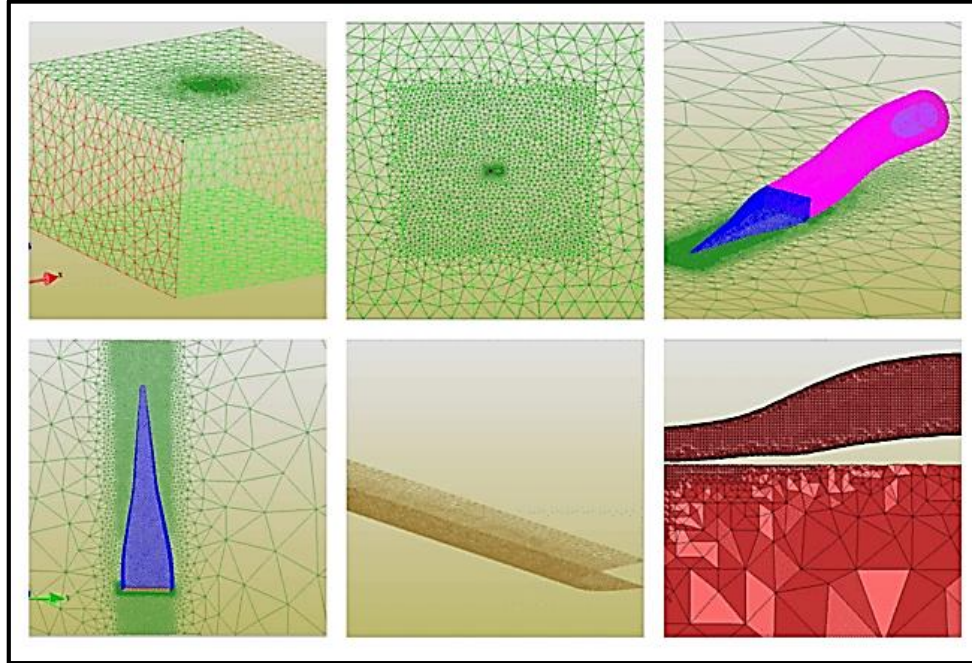| S/N	H(km)	Throttle	Mass Flow Rate (kg/s)	Mach Number	Velocity (m/s)
1		Max		0.2	67.3
2			6.65	0.4	126.6
3				0.6	189.9
4				0.85	289.2
5		Idle		0.2	67.3
6	Sea Level		4.55	0.4	126.6
7				0.6	189.9
8				0.85	289.2

Table 3: Flight Envelope

Figure11: Mesh Profiles

4. Solver

The solver used is Pressure based compressible solver which solves Navier-Stokes equations. The governing equations are as follows: -

$$\frac{\partial U}{\partial t} + \frac{\partial F}{\partial x} + \frac{\partial G}{\partial y} + \frac{\partial H}{\partial z} = J \qquad (4)$$

Where U, F, G, and H are flux variables

$$U = \begin{Bmatrix} \rho \\ \rho u \\ \rho v \\ \rho w \\ \rho \left(e + \frac{v^2}{2} \right) \end{Bmatrix} \quad (5)$$

$$F = \begin{Bmatrix} \rho u \\ \rho u^2 + p - \tau xx \\ \rho vu - \tau xy \\ \rho wu - \tau xz \\ \rho \left(e + \frac{v^2}{2} \right) u + pu - k\frac{\partial T}{\partial x} - u\tau xx - v\tau xy - w\tau xz \end{Bmatrix} \quad (6)$$

$$G = \begin{Bmatrix} \rho v \\ \rho uv - \tau yx \\ \rho v^2 + p - \tau yy \\ \rho wv - \tau yz \\ \rho \left(e + \frac{v^2}{2} \right) w + pv - k\frac{\partial T}{\partial y} - u\tau yx - v\tau yy - w\tau yz \end{Bmatrix} \quad (7)$$

$$H= \left\{ \begin{array}{c} \rho w \\ \rho uw - \tau zx \\ \rho vw - \tau zy \\ \rho w^2 + p - \tau zz \\ \rho \left(e + \frac{v^2}{2} \right) w + pw - k\frac{\partial T}{\partial z} - u\tau xz - v\tau zy - w\tau zz \end{array} \right\} \quad (8)$$

Solver Settings and Boundary Conditions have been represented in Tables 4 and Table 5 respectively.

Parameter	Condition
Free stream Velocity	0.4 M
Angle of attack	0 degree
Total temperature	293 K
Free stream Static Pressure	101325 N/m^2
Mass Flow Rate	6.65 kg/s
Simulation Type	Steady State
Turbulence Model	2 eq. k-ε turbulence model

Table 4: Solver Settings

Boundary	Boundary Conditions
Domain	Subsonic Inflow, Static Pressure 101325 N/m2, Static Temperature 288.15 K, flow direction normal to the boundary
Engine Face	Mass flow rate = 6.65 kg/s
NACA Duct, S Duct, Inlet Lip, Engine Hub	Viscous Adiabatic Wall, No-slip Condition

Table 5: Boundary Conditions

To calculate the above-mentioned boundary conditions, META-COMP CFD++ software has been used. 1000 iterations and order of magnitude convergence up to 10-5 are applied.

5. Losses in an Intake

Intake is no different from any other existing engineering system where a fraction of the supplied energy goes to waste i.e., it is spent in ways other than desired. The following could be the probable reasons for the losses: -

- Friction on the walls of the duct
- Turbulent mixing and vortex generation
- Flow separation due to adverse pressure gradient as well as bends.
- Flow distortion
- Shockwaves

6. Factors affecting Performance of Air Intake

6.1 Total Pressure Loss

The air intake duct either diffuses free stream air from a high inlet Mach number to a low Mach number (as in the case of UAV cruising at high speed) or accelerates the free stream air from static condition to an acceptable level of compressor inlet Mach number (as in the case of UAV takeoff). In either case, the air stream suf-

fers a total pressure loss through intake due to some or all of the reasons listed above. Intake duct pressure can be written in terms of the following parameters only:

(i) Duct Geometry- loss due to geometry is accounted for as a loss coefficient, usually called lambda, λ

(ii) Inlet Mach number or dynamic head.

(iii) Inlet swirl angle
Total pressure loss in terms of λ is defined in Eq. 10:
Pin – Pout = λ (Pin – PSin) (10)
Where,

Pin – Total Pressure at the entry of duct Pout – Total Pressure at the duct exit
PSin – Static Pressure at the entry of the duct
The loss coefficient λ is the fraction of dynamic head lost in the duct, whatever the level of Mach number. Its magnitude is a fraction of only duct geometry and inlet swirl angle. Total pressure loss concerning inlet Mach number can be determined initially by expressing inlet dynamic head divided by inlet total pressure as a function of inlet total to static pressure ratio.

6.2 Pressure Recovery

Pressure recovery factor (PRF) is a commonly utilized parameter in the design of conventional turbojet intakes to assess how effectively the intake delivers air from ambient static pressure to a target AIP static pressure. It is defined as the ratio of the AIP's total pressure to that of upstream infinity. It is described mathematically in Eq. 11.

$$\eta PR = P2/P0 \tag{11}$$

Pressure recovery is affected by two losses viz. skin friction and turbulent mixing. Pressure recovery is a measure of loss in the intake flow with respect to the isentropic flow. The effect of intake pressure loss on engine thrust depends on the characteristics of the engine. Intake pressure loss can be assumed to be translated directly to the engine by the relationship indicated in Eq. 12.

$$X = K \left(\Delta P/P0\right) \tag{12}$$
Where,

ΔX – loss in thrust X – Thrust

K – a factor depends on the type of engine, generally, $1 < K \sim 1.5$

ΔP – Total Pressure loss at the intake exit P0 – Free stream total pressure

For flow speeds in the range of Mach number 0.5 to 1, the above equation can be roughly approximated as described in Eq. 13.

$$X = 0.35 \, KM0 \left(\Delta P/q\right) \tag{13}$$

Where M0 is the free stream Mach number and 'q' is free stream dynamic pressure. It is evident from the above equations that the loss in engine thrust is almost directly proportional to the intake pressure loss.

6.3 Circumferential Pressure Distortion

The circumferential ring pressure distortion index is based on the calculation of DP/PCring i, where the subscript "ring i" refer to any of the five pressure rings. The rings are counted in ascending order, outermost to innermost. The mathematical relationship is described in Eq. 14.

$$DP/PCring \; i = \{[PAVring \; i - PMINring \; i]/PA\} \text{ for rings } i = 1, 5 \tag{14}$$

All kinds of intake distortions are felt at the AIP and would severely affect the compressor's performance. To calculate the pressure distortion the geometry of points indicated in Fig. 12 and Fig. 13 had been introduced in front of the engine face:-
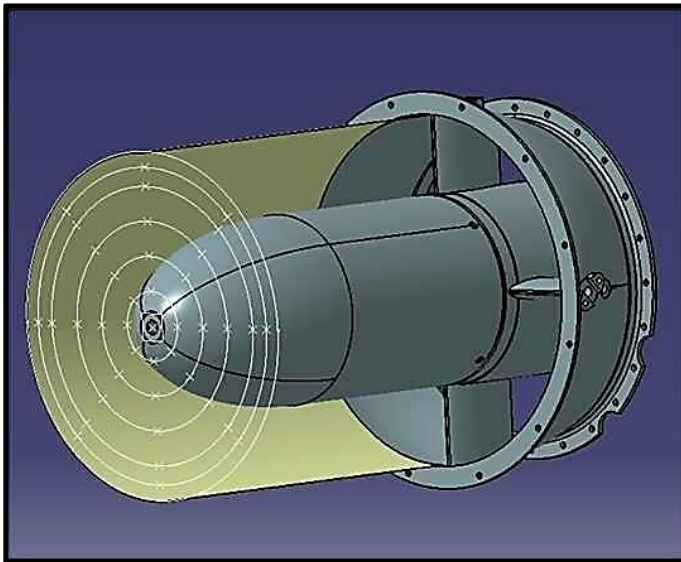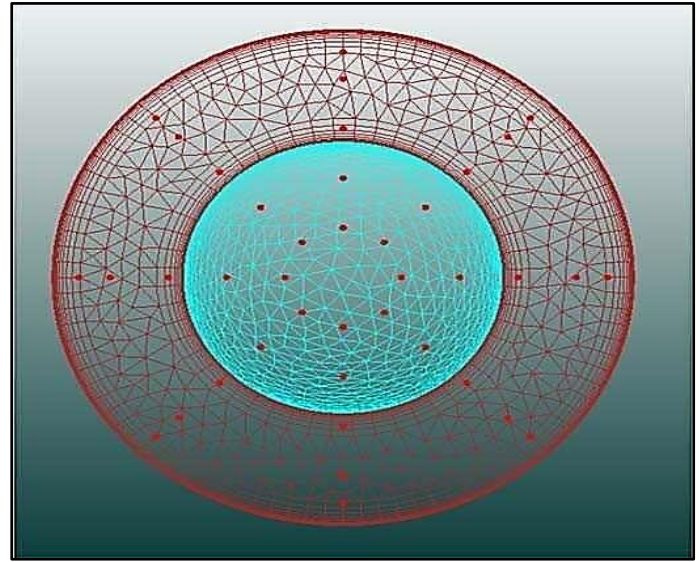

Figure12: Geometry of Pressure Points

Figure 13: Pressure Points in CFD++

Five rings have been introduced in the aforementioned drawings, with radii of 28.6 mm, 57.2 mm, 85.8 mm, 114 mm, and 130 mm. Eight evenly spaced points have been plotted on each ring to get the average total pressure there. The airflow may be deformed by the inlet when it is carried from the free stream to the compressor's face. As the air is brought from the free stream to the compressor's face, the flow may be distorted by the inlet. At the compressor face, one portion of the flow may have a higher velocity or higher pressure than another portion. The flow may be swirling, or some section of the boundary layer may be thicker than another section because of the inlet shape. The rotor blades of the compressor move in circles around the central shaft. The flow environment

around the blades rapidly alters as the blades meet distorted inlet flow. The compressor may stall, experience flow separation, or experience structural issues with the compressor blades as a result of changing flow conditions. High-pressure recovery and minimal distortion are qualities of a good intake.

7. Results

7.1 Static Pressure Distortion
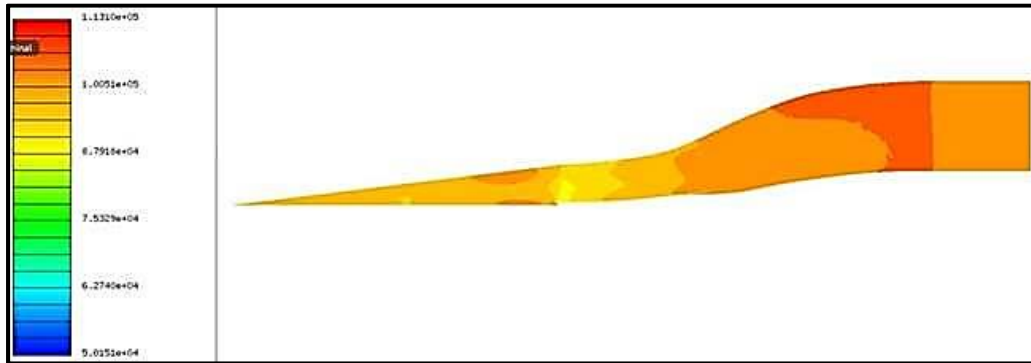Fig. 14 and Fig. 15 show the static pressure distribution at an inlet velocity of 0.4 M.

Figure14: Static Pressure Distribution over S Duct at 0.4 M
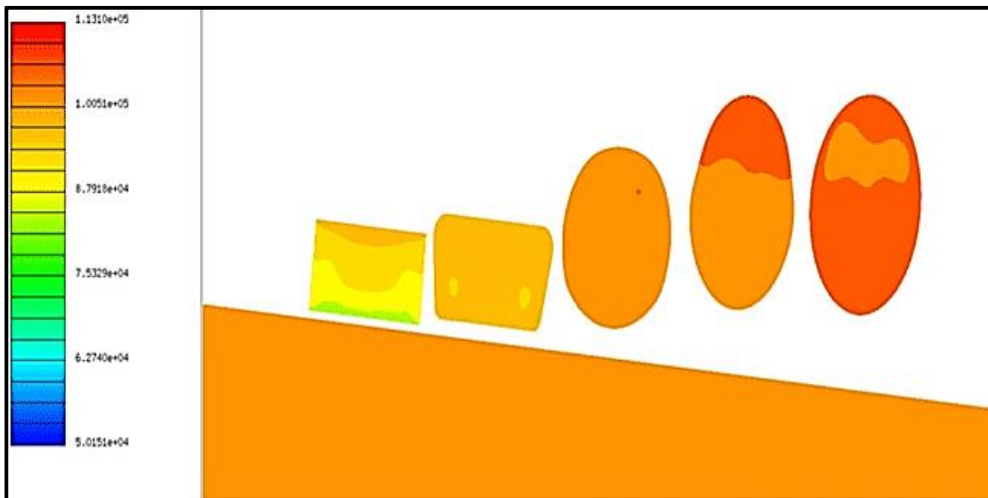
Figure 15: Static Pressure Distribution at cut planes (0.4 M)

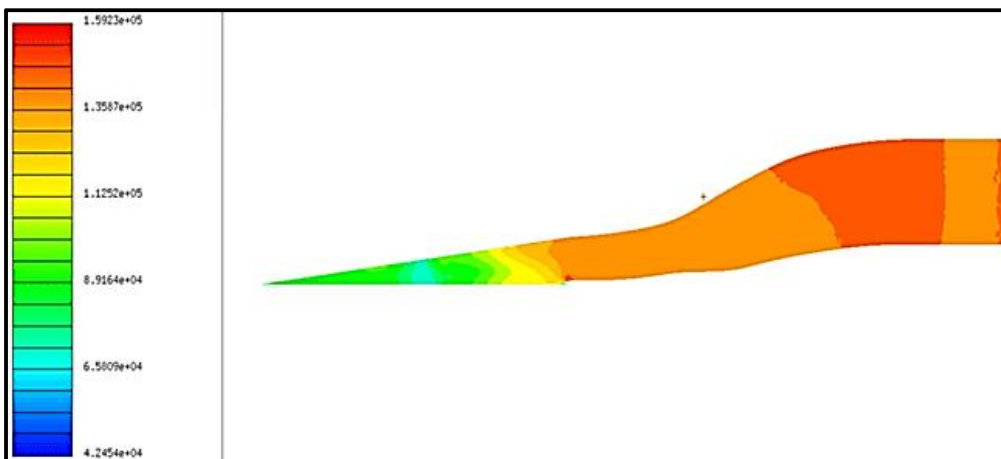Fig.16 and Fig. 17 show the static pressure distribution at an inlet velocity of 0.85 M

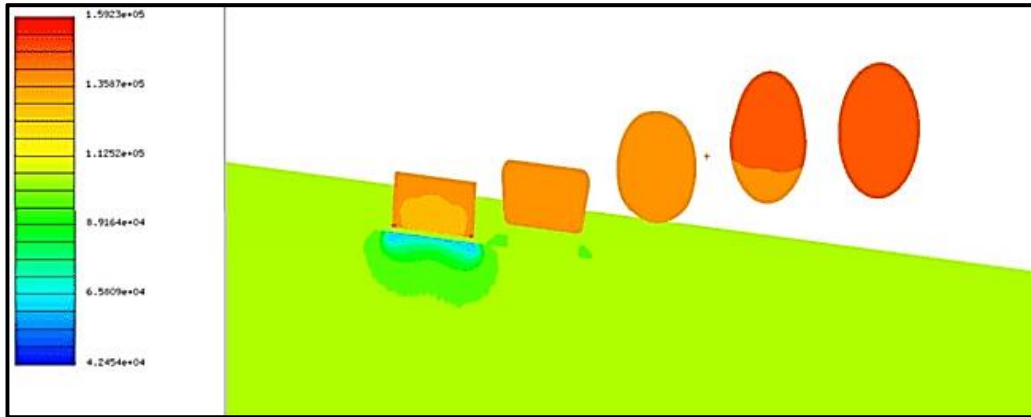**Figure 16:** Static Pressure Distribution over S-Duct at 0.85 M

Figure 17: Static Pressure Distribution at cut planes (0.85 M)

a. Mach Number Distribution

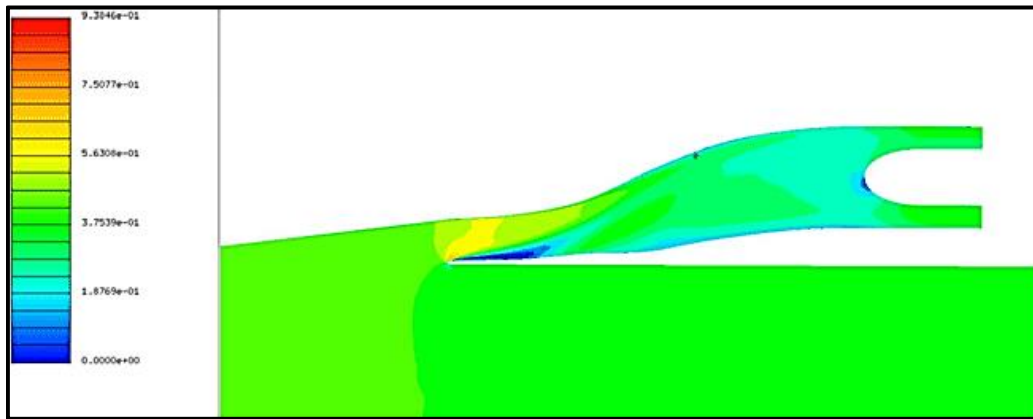Fig. 18 and Fig. 19 show Mach Number Distribution over the duct for an inlet velocity of 0.4 M.

Figure 18: Mach number Distribution over S-Duct at 0.4 M
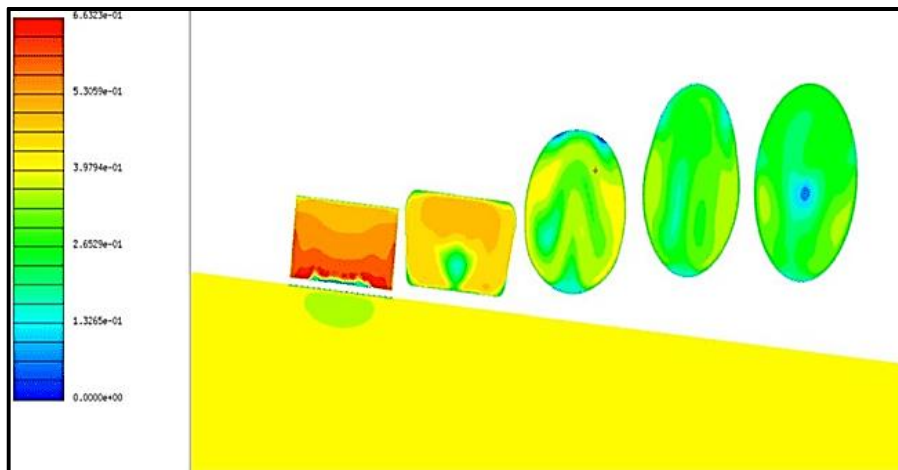

Figure 19: Mach Number Distribution at cut planes (0.4 M)

Fig. 19 and Fig. 20 show Mach Number Distribution over the duct for an inlet velocity of 0.85 M.
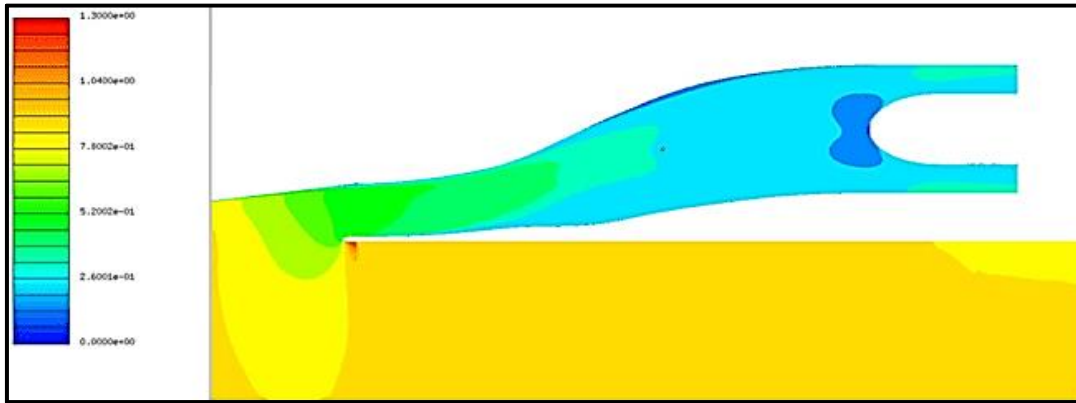
Figure 19: Mach Number Distribution over S-Duct at 0.85 M
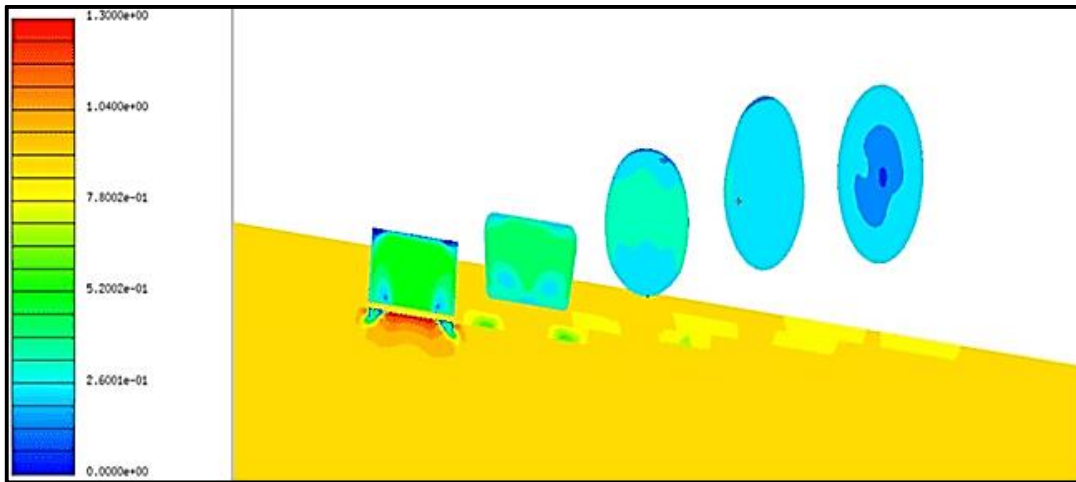

Figure 20: Mach Number Distribution at cut planes (0.85 M)

b. Flow Velocity Vectors at Engine Face

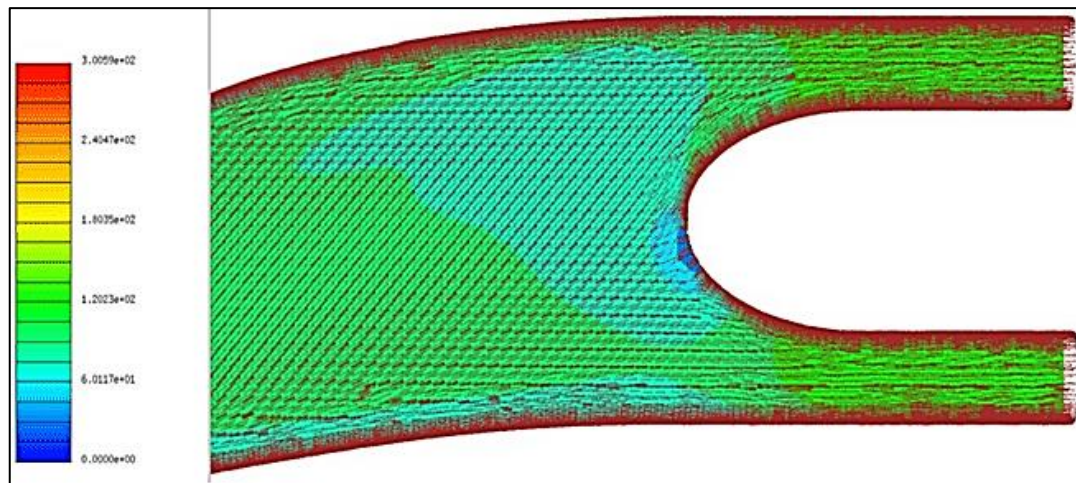Fig. 20 and Fig. 21 show the velocity vectors at the engine face.
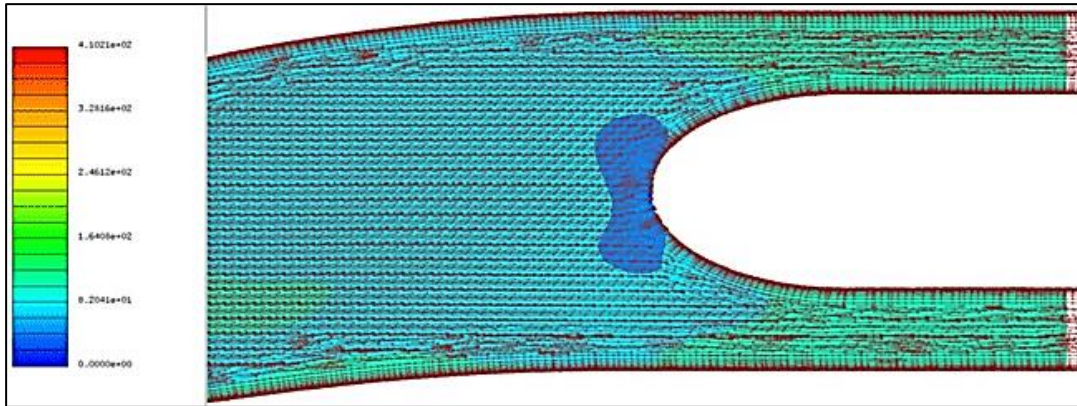

Figure 20: Flow Streamlines at 0.4 M

Figure 21: Flow Streamlines at 0.85 M

7.3 Pressure Distortion Data

Data for pressure distortion and pressure recovery for the cases of input velocities of 0.4 M, 0.6 M, and 0.85 M are presented in Table 6.

M (inlet)	Radius (mm)	Avg. P0 ring (bar)	P0 ring Min. (bar)	Avg. $P0_{engine}$ (bar)	P0 FS (bar)	DP/PC_{ring}	DP/PC	DP/PC_{max}	PRF
0.4	28.6	108530	107907	109251	113135	0.0057	0.0108	0.0176	96.6
	57.2	108854	107112			0.0159	0.0176		
	85.8	109624	107511			0.0193	0.0153		
	114.4	110316	109086			0.0113	0.0165		
	130	110548	108170			0.0218			
0.6	28.6	125201	124431	125856	129240	0.0061	0.0079	0.0188	97.4
	57.2	124273	123052			0.0097	0.0096		
	85.8	125916	124732			0.0094	0.0124		
	114.4	127347	125416			0.0153	0.0188		
	130	127119	124326			0.0222			
0.85	28.6	148492	148101	150471	162507	0.0026	0.0038	0.0058	92.6
	57.2	148235	147488			0.0050	0.0058		
	85.8	148654	147647			0.0067	0.0054		
	114.4	150183	149576			0.0040	0.0042		

From Fig. 14 - 20, it can be observed that through the diffusing shape of the duct, there is a rise in the magnitude of static pressure and a decrease in the velocity of the air, to make the flow conditions favorable for the compressor. With an increase in Mach number, there is also an increase in static pressure inside the duct. There is a smooth transition of the pressure gradient between the walls of the duct. From Fig. 19 a clear effect of Gerlach Shaping on the flow inside the duct can be seen. In Fig. 9, we can see that the area variation spline changes its curvature and the duct area gets increased exponentially after 50% length of the duct. The effect of this exponential change in area is reflected in CFD as one can see the "red" colored part (Fig. 14 and Fig. 16) at 75% length in all

cases is present in all most the same fashion. This shows the effect of Gerlach Shaping on static pressure distribution over the duct. From Fig. 20 and Fig. 21, it can be seen that the flow vectors are pretty straight when they go inside the compressor, which means that Gerlach Shaping is helping in restricting the formation of the secondary vortex flow generation inside the duct. Overall, Gerlach Shaping was found to be a good choice and the duct can deliver the desired flow characteristics in the conditions simulated. The Pressure Recovery Factor (PRF) is 96% at an inlet flow velocity of 0.4 M, 97.4% at 0.6 M, and 92.6% at 0.85 M. Pressure Recovery Factor is reduced at 0.85 M due to supersonic effects. Since the thrust generated by the engine is directly proportional to the pressure recovery factor, the UAV will be most efficient when it flies at speed of 0.6 M.

Conclusion

A submerged air intake system was designed within a pre-specified volume of fuselage available. The goal of this project was to get a foundation for future design iterations. Since the UAV has to be stealthy, no part of the system could go outside of the fuselage, hence a NACA Flush Inlet was chosen. The area required for the NACA inlet to pass the amount of mass flow required by the engine was calculated from the empirical ratios. A serpentine duct was chosen to deliver the air from the inlet to the engine. The Gerlach –Shaped design was adopted in order to decrease the strength of secondary vortices inside the S-Duct, which proved to be a good choice. After the designing process, the duct was analyzed over a range of flight conditions using CFD++ software. Parameters like Pressure Recovery Factor and Circumferential Pressure Distortion were calculated to evaluate the design. In the CFD Data, it can be seen that the velocity is increased at the outer wall and decreased at the inner wall of the first bend and vice versa in the following turn, thus reducing the pressure gradient between the walls. The maximum pressure recovery factor is found to be 97.4% at a velocity of 0.6 M. The initial requirement to get a mass flow rate of 6.65 kg/s is achieved. The engine is getting a streamlined flow of velocity between 0.3-0.4 M in all conditions. However, at low flight speeds, there is a little drop in the pressure recovery factor due to the length of the duct. The initial design proved to be sufficient. Some fine-tuning in the length and shape of the duct will decrease the losses due to duct geometry after which excellent numbers for the parameters analyzed can be obtained.

References

1. Haines, A. B. (2000). Intake Aerodynamics—Second edition. J. Seddon and EL Goldsmith. Blackwell Science, Osney Mead, Oxford OX2 0EL, UK. 1999. 1407pp. Illustrated.£ 59.50. ISBN 0-632-04963-4. The Aeronautical Journal, 104(1032), 96-96.
2. Towne, C., & Schum, E. (1985, July). Application of computational fluid dynamics to complex inlet ducts. In 21st Joint Propulsion Conference (p. 1213).
3. Gupta, V., Devpura, R., Singh, S. N., & Seshadri, V. (2001). Effect of aspect ratio and curvature on characteristics of S-shaped diffusers.
4. Menzies, R. D. (2002). Investigation of S-shaped intake aerodynamics using computational fluid dynamics (Doctoral dissertation, University of Glasgow).
5. Berrier, B., & Allan, B. (2004, January). Experimental and computational evaluation of flush-mounted, S-duct inlets. In 42nd AIAA aerospace sciences meeting and exhibit (p. 764).
6. Gopaliya, M. K., Kumar, M., Kumar, S., & Gopaliya, S. M. (2007). Analysis of performance characteristics of S-shaped diffuser with offset. Aerospace Science and Technology, 11(2-3), 130-135.
7. Lee, J., & Cho, J. (2018). Effect of aspect ratio of elliptical inlet shape on performance of subsonic diffusing S-duct. Journal of Mechanical Science and Technology, 32, 1153-1160.
8. Seddon, J., & Goldsmith, E. L. (1985). Intake aerodynamics. AIAA education series, New York.
9. Papadopoulos, F., Valakos, I., & Nikolos, I. K. (2012). Design of an S-duct intake for UAV applications. Aircraft Engineering and Aerospace Technology, 84(6), 439-456.
10. Raymer, D. (2012). Aircraft design: a conceptual approach. American Institute of Aeronautics and Astronautics, Inc.